Chapter 1
Nanoscale Characterization of Multiferroic Materials

Jan Seidel and Ramamoorthy Ramesh

Abstract Research on multiferroic materials over the last years has greatly benefitted from new developments and advanced methodology in characterization, such as scanning probe microscopy (SPM), X-ray diffraction (XRD) and synchrotron-based X-ray spectroscopy and microscopy techniques such as X-ray absorption (XAS) and X-ray circular and linear magnetic dichroism combined with photoelectron emission microscopy (XMCD- and XMLD-PEEM), Raman spectroscopy, second-harmonic generation (SHG), neutron scattering, transmission electron microscopy (TEM), and Mössbauer spectroscopy, to name only the more common ones. All these techniques have been applied in the study of multiferroics to extract critical information and give new insights on various length scales, including the nanoscale. In this chapter we present a general overview over major experimental techniques to characterize multiferroic materials.

Chapter in "*Mesoscopic Phenomena in Multifunctional Materials*" edited by A. Saxena and A. Planes (Springer, 2014)

J. Seidel (✉)
School of Materials Science and Engineering, University of New South Wales, Sydney, Australia
e-mail: jan.seidel@unsw.edu.au

R. Ramesh
Materials Sciences Division, Lawrence Berkeley National Laboratory, Berkeley, CA, USA
e-mail: rramesh@berkeley.edu

R. Ramesh
Department of Physics, University of California at Berkeley, Berkeley, CA, USA

R. Ramesh
Department of Materials Science and Engineering, University of California at Berkeley, Berkeley, CA, USA

R. Ramesh
Oak Ridge National Laboratory, Oak Ridge, USA

A. Saxena and A. Planes (eds.), *Mesoscopic Phenomena in Multifunctional Materials*, Springer Series in Materials Science 198, DOI: 10.1007/978-3-642-55375-2_1,

Transition metal oxides exhibit a rich physics resulting in a wide variety of properties that are related to a delicate balance between charge, spin and orbital degrees of freedom [1]. There has been a large body of work on these materials, mainly on members of the perovskite family, which offer the advantage of very high structural quality growth. Typical synthesis methods such as pulsed laser deposition (PLD), molecular beam epitaxy (MBE) and metal-organic chemical vapor deposition (MOCVD), among others, are now highly developed to engineer complex transition metal oxides with atomic-scale precision. This degree of control, e.g. allows for the study of heterointerfaces between a large variety of different materials. Such interfaces locally break the symmetry, induce stress, and vary the bonding between ions. This in turn gives rise to changes in bandwidth, orbital interactions and level degeneracy, opening venues for modifying the electronic structure of these strongly correlated materials.

Many transition metal oxides are ferroics, i.e. materials with a spontaneous, reversible ordering. Ferroic phases can arise in two or more distinct orientations of the order parameter, i.e. they can form domains, separated by domain walls. Domains are a representation of long-range order with respect to at least one macroscopic tensor property of the material (order parameter). When orientation states are changed, the interfaces (domain walls) move; thus the domain structure can be manipulated by external fields, which is a central feature of ferroic materials. In general, in the vicinity of such a transition one or more macroscopic properties of the material associated with the order parameter can become large and very susceptible to external fields. Field-induced phase transitions around the transition temperature are a common feature. Subsets of ferroic phase transitions are ferroelectric, ferroelastic and ferromagnetic transitions. These involve the emergence of spontaneous polarization, spontaneous strain, or spontaneous magnetization and are commonly referred to as primary or first order ferroics. Many so-called smart materials and structures have at least one of these properties and are designed to change them in a preconceived manner through the application of external fields. Multiferroics are defined as materials that have at least two of these ferroic properties: ferromagnetism, ferroelectricity, ferroelasticity, or ferrotoroidicity (or their antiferroic counterparts, e.g. antiferromagnetism).

A large amount of research has been dedicated to magnetoelectric multiferroics (Fig. 1.1). In these materials magnetic or electric polarization can be induced by applying an external electric or magnetic field [1, 2]. In such materials there is the possibility that electric fields cannot only reorient the polarization but also control magnetization at the same time. The main objective here is to combine ferroelectricity with ferromagnetism or with other types of magnetism, i.e. ferri- and antiferromagnetism. The same properties can also be found in artificial heterostructures (or interfaces) such as ferroelectrics stacked with magnetic materials and ferromagnets embedded in ferroelectric hosts [5]. These properties are interesting for electric-field control of magnetism which is a pathway to smaller, more energy-efficient devices. One key aspect to realize the application of multiferroics into novel device architectures depends on the basic understanding of the material systems and their rigorous characterization by various methods.

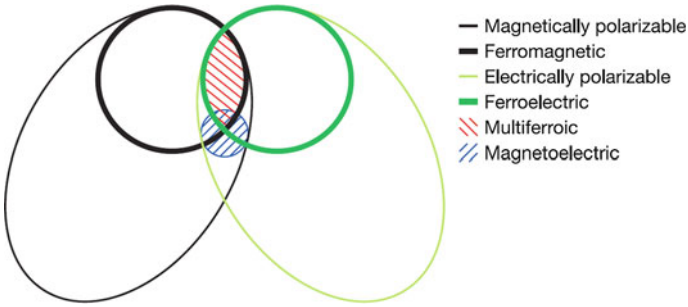

Fig. 1.1 Magnetic, ferroelectric, multiferroic and magnetoelectric materials. From [2]

Multiferroic materials characterization relies on advanced methodologies, such as scanning probe microscopy (SPM), X-ray diffraction (XRD) and synchrotron-based X-ray spectroscopy and microscopy techniques such as X-ray absorption (XAS) and X-ray circular and linear magnetic dichroism combined with photo-electron emission microscopy (XMCD- and XMLD-PEEM), Raman spectroscopy, second-harmonic generation (SHG), neutron scattering, and transmission electron microscopy (TEM), and Mössbauer spectroscopy, to name only the more common ones. All these techniques have been applied in the study of multiferroics to extract critical information on various length scales, including the nanoscale. In the following we will provide specific examples on how these techniques have been used to characterize multiferroic materials.

1.1 Scanning Probe Microscopy: Nanoscale Transport and Electronic Structure

Scanning Probe Microscopy (SPM) with all its variations (e.g. conductive-AFM, PFM) are very well suited for the direct characterization of prototype multiferroic materials, including their interfaces [3]. Charge transfer can induce carrier densities that are different at these interfaces than in the bulk, resulting in physical properties at the interface which may be completely different from those of the parent bulk materials [4–8]. The recent development of specialized local scanning probe based measurements now allows for nanoscale probing of these interfaces between strongly correlated oxides. Tuning and controlling the physical properties of these interfaces between different oxide materials provides a new playground for research and offers a new nanoelectronics characterization platform for future nanotechnology [9].

With conductive AFM (c-AFM) one can probe local conductivity at interfaces and topological defects which are of concern to ferroelectric capacitor based applications. Piezoresponse force microscopy (PFM) is also under continuous development, and is currently undergoing a shift of focus from imaging static

domains to dynamic characterization of the switching process (with developments such as stroboscopic PFM and PFM spectroscopy) [10–13]. Multiferroic thin films typically contain various structural defects such as cationic and/or anionic point defects, dislocations and grain boundaries. Since the electric and stress fields around such defects in a ferroelectric thin film are likely to be inhomogeneous, it is expected that the switching behavior near a structural defect will be different from the one found in a single domain state. The role of a single ferroelastic twin boundary has been studied e.g. in tetragonal $PbZr_{0.2}Ti_{0.8}O_3$ ferroelectric thin films [14]. It was shown that the potential required to nucleate a 180° domain is lower near ferroelastic twin walls. A recently increased interest in local conductivity measurements arises from both non-volatile memory application perspective and a potential for electroresistive memory devices [15] and are also interesting for the characterization of oxygen vacancy movement and ionic battery materials on the nanoscale [16, 17]. In many cases, the presence of extended defects and oxygen vacancy accumulation makes the identification of polarization mediated transport mechanisms difficult, although direct probing of polarization-controlled tunneling into ferroelectric surfaces has been demonstrated [18, 19]. The combination of local electromechanical and conductivity measurements has revealed a connection between local current and pinning at bicrystal grain boundaries in bismuth ferrite [20]. Electroresistance in ferroelectric structures has recently been reviewed by Watanabe [21]. The presence of extended defects and oxygen vacancy accumulation has been shown to influence transport mechanisms at domain walls [22, 23]. Recently, direct probing of polarization-controlled tunneling into ferroelectric surface has been shown. Scanning-near-field optical microscopy (NSOM) has been used to observe pinning and bowing of a single ferroelectric domain wall under a uniform applied electric field [24, 25]. Scanning microwave microscopy has been applied to the study of mesoscopic metal-insulator transition at ferroelastic domain walls in VO_2 [26, 27].

Scanning tunnelling spectroscopy can be used to probe directly the superconducting order parameter at nanometer length scales. Scanning Tunneling Microscopy (STM) and spectroscopy (STS) have been used to investigate the electronic structure of ferroelastic twin walls in $YBa_2Cu_3O_{7-\delta}$ [28]. Twin boundaries play an important role in pinning the vortices and thereby enhancing the currents that oxide superconductors can support while remaining superconducting. An unexpectedly large pinning strength for perpendicular vortex flux across such boundaries was found, which implies that the critical current at the boundary approaches the theoretical ‘depairing’ limit. In the case of insulators, STM/STS are by definition a lot more difficult to implement, primarily because a reliable tunnelling current cannot be used to establish proximal contact. The emergence of ferroelectrics with smaller bandgaps and the possibility of conduction at domain walls (see later) has stimulated renewed interest in exploring STM as a probe of the local electronic structure. The emergence of combined AFM/STM or SEM/STM systems should be a boon in terms of exploring the electronic properties of domain walls in such insulating materials. Research using such combined tools is in its infancy [29–32].

The changes in structure (and as a consequence electronic structure) that occur at multiferroic domain walls can lead to changes in transport behavior. Indeed, domain wall conductivity has been shown in different ferroic materials, although with different transport behavior: the domain walls of $BiFeO_3$ were found to be more conductive than the domains (Fig. 1.2), [22] while those of hexagonal manganites (e.g. Er MnO_3) were found to be more insulating or conductive depending on their orientation [33, 34]. Multiferroic $YMnO_3$, a so-called improper ferroelectric multiferroic, in which ferroelectricity is induced by structural trimerization coexisting with magnetism, domain walls are found to be charged and stable. This material exhibits a conductive 'cloverleaf' pattern of six domains emerging from one point, and the ferroelectric state has been reported to be more conducting than the paraelectric state.

The role of defect accumulation at these domain walls and the control of the electronic structure at walls by doping and strain also deserves close investigation by scanning probe microscopy. For the case of $BiFeO_3$ A-site doping with Ca, and magnetic B-site substitution such as Co or Ni, might prove to be a viable way to achieve new domain wall properties by manipulating the electronic structure, spin structure, and dipolar moment in this material [15]. Localized states are found in the spectrum of ferroelectric semiconductors, and states localized at the walls and inside the domain but close to the wall split off from the bulk continuum. These nondegenerate states have a high dispersion, in contrast with the "heavy-fermion" states at an isolated domain wall [35]. Charged double layers can be formed due to coupling between polarization and space charges at ferroelectric-ferroelastic domain walls [36]. Charged domain wall energies are about one order larger than the uncharged domain wall energies [37], and phenomenological calculations show decoration of walls by defects such as oxygen vacancies. The presence of charge and defect layers at the walls means that such walls promote electrical failure by providing a high conductivity pathway from electrode to electrode [36].

Recently, the observation of tunable electronic conductivity at domain walls in La-doped BFO linked to oxygen vacancy concentration has been reported (see Fig. 1.3), [23]. Specific growth conditions have been used to introduce varying amounts of vacancies in thin film samples [38]. The conductivity at 109° walls in such samples is thermally activated with activation energies of 0.24 to 0.5 eV. From a broader perspective, these results are a first step towards realizing the tantalizing possibility of inducing an insulator-metal transition locally within the confines of the domain wall through careful design of the electronic structure, the state of strain and chemical effects at the domain wall. For actual device applications the magnitude of the wall current needs to be increased. The choice of the right shallow-level dopant and host material might prove to be key factors in this respect. Further study of correlations between local polarization and conductivity are an exciting approach to understanding the conduction dynamics and associated ferroelectric properties in the presence of strong coupling between electronic conduction and polarization in complex oxides.

The concept of doping has also been applied to bismuth ferrite in an attempt to modify the electronic and magnetic properties and to reduce leakage currents [15, 39]. B-site doping of BFO with Ti^{4+} has been shown to reduce leakage by

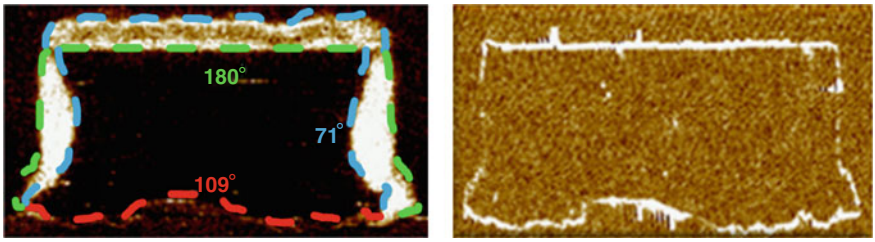

Fig. 1.2 The three different types of domain walls in rhombohedral bismuth ferrite. As seen in an in-plane PFM image of a written domain pattern in a mono-domain BFO (110) and corresponding c-AFM image showing conduction at both 109° and 180° domain walls

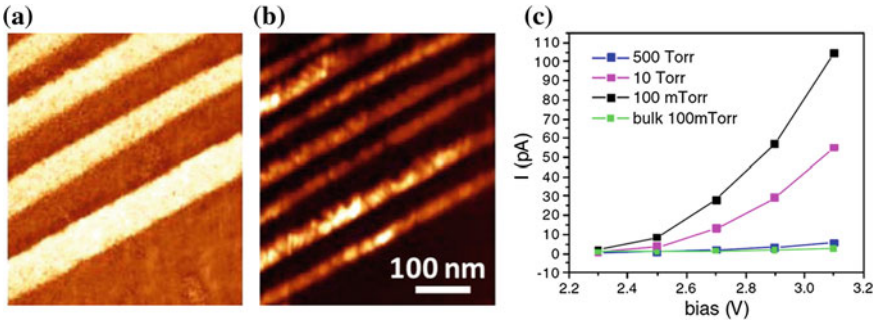

Fig. 1.3 **a** PFM phase images of a BFO sample with 109° stripe domains. **b** Simultaneously acquired c-AFM image of the same area showing that each 109° domain wall is electrically conductive. **c** Current levels for samples with different oxygen cooling pressure and thus varying density of oxygen vacancies

over three orders of magnitude while doping with Ni^{2+} leads to a higher conductivity by over two orders of magnitude [40]. Likewise, doping with Cr or Mn has also been shown to greatly reduce leakage currents in BFO films [41].

Yang et al. [15] (Fig. 1.4) investigated Ca doping of BFO with results showing strong similarity to phase diagrams of high-T_C superconductors and colossal magnetoresistive manganites where a competition between energetically similar ground states is introduced by hole doping. Control of the conductive properties by band-filling was observed in Ca-doped BFO. Application of an electric field enabled this control to the extent that a p–n junction can be formed, erased and inverted in this material. A 'dome-like' feature in the phase diagram is observed around a Ca concentration of 1/8, where a new pseudo-tetragonal phase appears and the electric modulation of conduction is found to be largest. Conductive-AFM measurements reveal that the material exhibits resistive switching and that subsequent application of electric fields can reverse the effect. The observed reversible modulation of electric conduction accompanied by the modulation of the ferroelectric state is a consequence of the spatial movement of naturally produced oxygen vacancies under an electric field that act as donor impurities to compensate

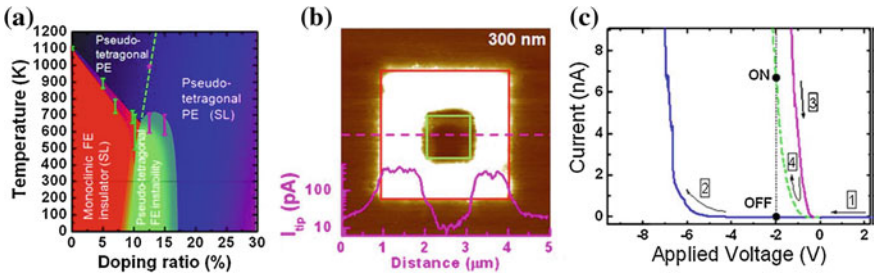

Fig. 1.4 Ca-doping of multiferroic $BiFeO_3$. **a** Phase diagram of Ca-doped $BiFeO_3$. **b** c-AFM image of an electrically poled and re-poled area of the doped $BiFeO_3$ film. The electrically poled area (*white area*) has become conducting. **c** I–V curve acquired during the switching process. Adapted from Yang et al. [15]

Ca acceptors and maintain a highly stable Fe^{3+} valence state. This observation might lead to new concepts for merging magnetoelectrics and magnetoelectronics at room temperature by combining electronic conduction with electric and magnetic degrees of freedom [42–44].

Another area of scanning probe based investigation is the study of light-matter interactions in multiferroics. Recently, an anomalous photovoltaic effect in multiferroic BFO thin films has been found which arises from a unique, new mechanism—structurally driven steps of the electrostatic potential at nanometer-scale domain walls [45–47]. In conventional solid-state photovoltaics, electron–hole pairs are created by light absorption in a semiconductor and separated by the electric field spanning a micrometer-thick depletion region. The maximum voltage these devices can produce is equal to the semiconductor electronic bandgap. Interestingly, domain walls can give rise to a fundamentally different mechanism for photovoltaic charge separation, which operates over a distance of 1–2 nm and produces voltages that are significantly higher than the bandgap. Recent investigations using conductive AFM under light illumination reveal these high photovoltages at 71° and 109° domain walls in BFO (see Fig. 1.5), [47]. Electric-field control over domain structure allows the photovoltaic effect to be reversed in polarity or turned off.

STM and STS measurements in cross-sectional samples have also been used to directly investigate the nature of the unusual local electronic conductivity at ferroelectric domain walls in multiferroic BFO [32]. In situ cleaved samples with ordered stripe arrays show a decrease of the bandgap at the domain boundaries. In addition, a shift towards the Fermi level in the band edges of 109° and 71° domain walls have been measured (Fig. 1.6). The demonstrated approach in this work serves as a model technique to investigate and understand electronic structure at oxide interfaces.

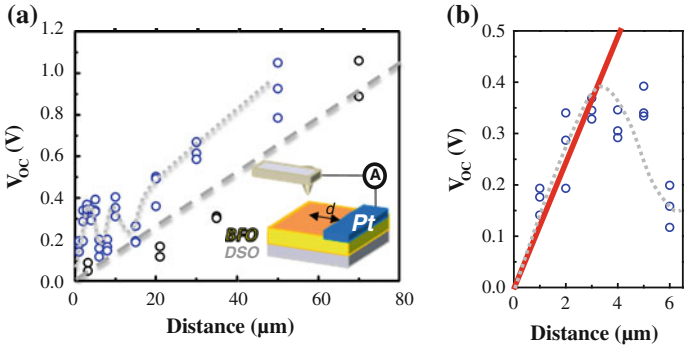

Fig. 1.5 Local measurements of V_{OC}. **a** 109° domain walls (*blue*) show different, oscillating behavior of V_{oc} with distance as compared to 71° domain walls (*black*). Inset: schematic nanoscale PV measurement setup using a conductive AFM tip as a variable-distance counter electrode for I–V characterization. **b** Initial large slope (*red line*) indicating large PV effect at 109° walls

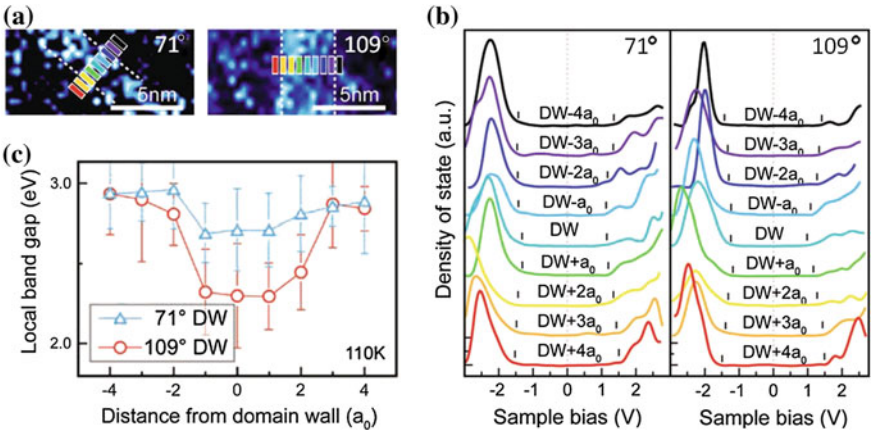

Fig. 1.6 Layer-by-layer dI/dV measurements across 71° and 109° domain walls in $BiFeO_3$ acquired at 110 K. Bars in **a** denote positions where the electronic spectra are probed, and **b** shows the corresponding STS spectra. The band edges are indicated by *black* tick marks in (**b**). **c** Extracted local band gap across the domain walls. Adapted from [32]

1.2 X-Ray Based Techniques: XRD, XAS and XMCD- and XMLD-PEEM

XRD has been widely employed to characterize the crystal structure of the materials, as well as probing the structural phase transitions. An interesting example of this can be found in mixed phase BFO [48–51]. Here epitaxial strain is used as a tool to create a new ground state of a material. Thin film growth on

$LaAlO_3$ substrates imposes a large compressive epitaxial strain which allows to stabilize a tetragonal-like phase (T-phase) with a significantly large c/a ratio. It was shown that partial relaxation of the epitaxial strain leads to the formation of a nanoscale mixture of the T- and rhombohedral R-phases, thus resembling a classical morphotropic phase boundary. XMCD-PEEM imaging has been used to explore the ferromagnetic properties of BFO films with mixed phases, and compared to unconstrained R-and pure T-phase films [52, 58].

Recently, temperature-dependent XRD reciprocal space mapping has been used to find the concurrent transition of ferroelectric and magnetic ordering near room temperature [53], see Fig. 1.7. Specifically it was shown that the magnetic Néel temperature of the multiferroic $BiFeO_3$ is suppressed to around room temperature by heteroepitaxial misfit strain in a highly elongated tetragonal-like phase (T-BFO). Remarkably, the ferroelectric state undergoes a first-order transition to another ferroelectric state simultaneously with the magnetic transition temperature, which provides a unique example of a concurrent magnetic and ferroelectric transition at the same temperature among proper ferroelectrics, taking a step toward room temperature magnetoelectric applications.

To understand why the highly elongated phase has the Néel temperature largely suppressed to near room temperature, the electronic state of the 3*d* levels should be clarified. Figure 1.8a displays a schematic representation of transition metal oxide local structures and site symmetries. According to the ligand field theory, the fivefold degenerated 3*d* level is split into triplet t_{2g} and doublet e_g levels in the octahedral (O_h) symmetry. The elongation of the octahedron along the *c*-axis reduces to the tetragonal (D_{4h}) symmetry and generates additional Jahn-Teller-type level splitting [54]. In the T-BFO phase, the elongation is extremely large and is accompanied with a large Fe shift along the *c*-axis to relieve the strong Coulombic repulsion between the Fe ion and neighbouring oxygen ions in the *ab* plane. As a result, the local structure becomes the FeO_5 pyramid in the C_{4v} site symmetry, where the in-plane *xy* orbital level becomes the lowest. This cation-shifted oxygen pyramidal structure is exactly what happens in the highly elongated T-BFO phase [53].

Experimental evidence of the pyramidal C_{4v} symmetry can be confirmed by polarization-dependent O *K*-edge XAS measurements, which directly show transferred O_{2p} partial density due to hybridization with the unoccupied orbital states. As seen in Fig. 1.8b, the spectra are roughly divided into Fe_{3d}, Bi 6 *sp* and Fe 4 *sp* orbital character regions for both R-BFO and T-BFO. In R-BFO, the spectrum does not vary much for the different incoming photon polarization (E∥ *c* and E∥ *a*) indicating that the orbital anisotropy is relatively small. In contrast, the O *K*-edge spectrum of T-BFO exhibits strong polarization dependence, particularly in the Fe 3*d* region, reflecting the strong orbital anisotropy, as also observed in the Fe *L*-edge linear dichroism. Taking advantages of the strict dipole selection rules in the polarization-dependent XAS (the E∥ *c* light enhances the absorption to the O_{2p} states hybridized with the out-of-plane $d_{yz/zx}$ and $d_{3z^2-r^2}$ orbitals whereas the E ⊥ *c* light does one to the O_{2p} states hybridized with the in-plane d_{xy} and $d_{x^2-y^2}$ orbitals), we can confidently identify the four distinguishable Fe 3*d* orbital states in the

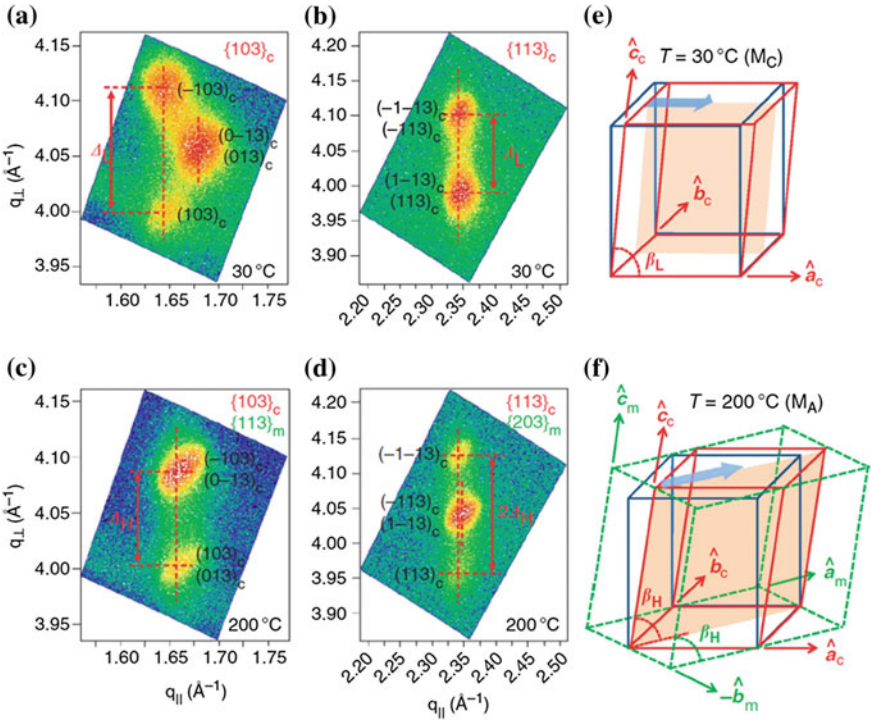

Fig. 1.7 Strained BFO thin film on $LaAlO_3$ crystal structure characterized by X-ray reciprocal space maps. **a** Pseudocubic {103} peaks at 30 °C. **b** {113} peaks at 30 °C. **c** {103} peaks at 200 °C. **d** {113} peaks at 200 °C. **e** The pseudocubic unit cell of the lower temperature phase has a monoclinic distortion where the *c*-axis direction tilts up toward [100]. **f** The pseudocubic unit cell at the higher temperature. In this case, the direction of the *c*-axis tilt is toward [110]. The high temperature structural phase is similar to the normal R-BFO film in terms of the direction of the distortion, however, it is apparently different in terms of the large *c*-axis lattice parameter. From [53]

conduction band as indicated in Fig. 1.8b. The identified 3*d* orbital level splitting exactly coincides with those in the pyramidal C_{4v} symmetry, including the lowest energy d_{xy} orbital state, whereas they are against the elongated tetragonal D_{4h} level splitting. These results experimentally provide strong spectroscopic evidence on the formation of the FeO_5 pyramid resulting from the highly off-centered Fe position in T-BFO.

Another example for detailed X-ray based investigations is the investigation of the phase diagram of the $Bi_{1-x}Ca_xFeO_{3-\delta}$ thin films as a function of the Ca doping concentration (x) and temperature through structural analysis [15, 55, 56]. For the low Ca doping regime ($x < 0.1$), films with a monoclinic structure undergo a first-order transition to a pseudo-tetragonal phase at higher temperatures with a thermal hysteresis. The extrapolation of the transition temperature results in the well-known ferroelectric Curie temperature (Tc) of $BiFeO_3$ at $\sim$1,100 K. With increasing Ca

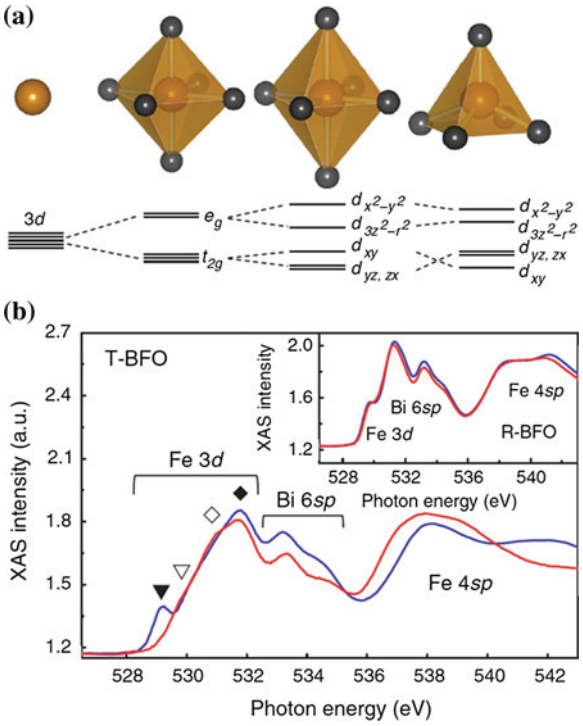

Fig. 1.8 Fe 3d level splits and O K-edge X-ray absorption spectra of tetragonal BFO (T-BFO). **a** Schematic representation of the transition metal oxide local structures and the 3d level splits in the spherical, octahedral (O_h), elongated tetragonal (D_{4h}) and square pyramidal (C_{4v}) site symmetries. In the highly elongated tetragonal case, the transition metal ion shifts along an apical direction for relief of the large Coulomb repulsion energy. This metal shift brings on the d_{xy} and d_{yz}/d_{zx} energy level switching. **b** Oxygen K-edge absorption spectra for different polarizations (E ∥ a (*blue line*) and E ∥ c (*red line*)) of T-BFO and R-BFO. In the T-BFO case, the spectrum exhibits large polarization dependence induced by the strong orbital anisotropy. (Inset) In the R-BFO case, the spectrum shows very small polarization dependence resulting from the weak orbital anisotropy. From [53]

doping, the ferroelectric T_c rapidly decreases, and a T_c of $\sim$600 K with a thermal hysteresis of 240 K is recorded at $x = 0.1$.

Zhao et al. [57] investigated the coupling between ferroelectricity and antiferromagnetism in BFO thin films by a combination of PFM and PEEM, which is based on the coupling of both antiferromagnetic and ferroelectric domains to the underlying ferroelectric domain switching. In another study, XMCD-PEEM was used to probe the interaction between ferromagnetic CoFe capping layers and BFO thin films to provide insights into the magnetoelectric coupling mechanism [58].

1.3 Probing Magnetism: Neutron Scattering and Mössbauer Spectroscopy

Neutron scattering has been used to investigate properties of multiferroics. It is an excellent method to investigate both structure and magnetic order. It has been applied to study the magnetic structure and the coupling between the ferroelectric and antiferromagnetic directions of multiferroic $BiFeO_3$. The recent developments in neutron sources and scattering techniques allow for in situ and/or time resolved investigations of multiferroic properties and non-destructive depth profiling in material systems, ideally suited for superlattice or heterostructure characterization. When neutrons are incident upon a sample, they interact with atomic nuclei and magnetic fields from unpaired electrons, unlike X-rays that probe only the electron cloud. The collisions involving the neutrons can be either elastic or inelastic. Examples of inelastic neutron scattering include neutron spin echo, neutron backscattering, time-of-flight scattering and triple-axis spectrometry. Both elastic and inelastic methods are well suited for the study of magnetism in multiferroics.

Neutron measurements on BFO crystals revealed that the antiferromagnetic sublattices show a cycloidal pattern with a period of 62 nm [59]. A change in the periodicity of this cycloid is observed when doping the A or B site with various metal ions or when BFO is mixed with $PbTiO_3$ [60, 61]. The cycloid leads to the canceling of the net magnetic moment resulting from canted sublattices, which explains the strongly increased interest in thin film BFO where the cycloid can be suppressed [62].

Recently, also the coupling between the ferroelectric and antiferromagnetic order was investigated for single crystals of BFO using neutron scattering shedding new light on magnetoelectric coupling in this material [63]. The single crystals in this study were designed to have only one as-grown ferroelectric domain. Lebeugle et al. measured the intensity distribution of the as-grown crystals around the four antiferromagnetic Bragg reflections of the (1/2, 1/2, 1/2) type before and after electric field poling in order to study the magnetic structure and magnetoelectric coupling of BFO. Prior to electric field poling the magnetic order is observed in only one direction whereas afterwards roughly half of the domains rotate by 71° demonstrating that the magnetic order is coupled to the ferroelectric order in BFO crystals (see Fig. 1.9). Ferroic domain switching and different forms of ME coupling have also been observed in other multiferroics using polarized neutron techniques [64–66].

Another interesting example of the advantage of using a neutron source for characterization of multiferroics involves the ability to measure the depth profile of magnetic properties using polarized neutron reflectometry, which can also be used for thin film materials. In this technique, a beam of neutrons is reflected (and refracted) from the sample and the intensity of the reflected beam is recorded at different neutron wavelengths and angles of incidence, which enables the collection of a chemical and magnetic depth profile through analysis of the change in the neutron momentum [67]. In summary, neutron based techniques offer many interesting insights into multiferroic materials.

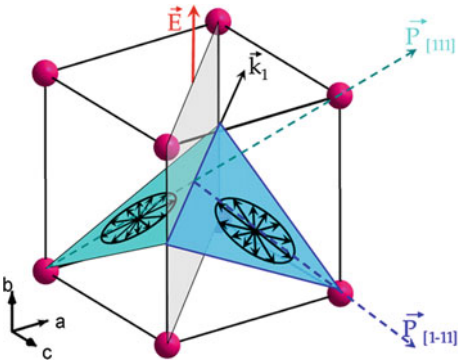

Fig. 1.9 Schematics representation of the planes of spin rotations and cycloids vector for the two polarization domains separated by a domain wall (in *light gray*) in bismuth ferrite. From [63]

Mössbauer spectroscopy has been used for example to determine the magnetic order in bismuth ferrite thin films grown under varying strain conditions [68]. This technique probes the hyperfine interactions between the nuclei and their electronic environment through the absorption of photons emitted by a radioactive source. During the experiments, the source is moved towards or away from the sample, which respectively blue- or red-shifts the radiation, thereby allowing for absorption in a very small energy range around the photon energy. The measured spectra provide information on the electronic density at the nuclei through the so-called isomer shift, a possible electric field gradient (quadrupole splitting) and the magnetic environment of the nuclei (magnetic splitting).

1.4 Optical Methods: Raman Spectroscopy and Second Harmonic Generation (SHG)

Raman spectroscopy and SHG are powerful tools to study ferroelectric and magnetic order in multiferroics, especially at surfaces and buried interfaces, which are hardly or not accessible by other techniques. For example, giant coupling of SHG to the spontaneous polarization in compounds with magnetically-driven ferroelectricity, such as $TbMn_2O_5$ has been observed [69]. Recently, electric-field controllable magnonics (spin waves) has been realized in multiferroic $BiFeO_3$ at room temperature by probing with Raman spectroscopy [12]. However, ferroics typically show complex domain structures and most of these techniques do not offer the spatial resolution to probe multiferroicity in nanoscale regions, especially in thin films. This is important for example in the investigation of magnetoelectric multiferroics for device applications [58].

In bismuth ferrite strong spin phonon coupling to the antiferromagnetic phase transition has been observed by Raman spectroscopy (see Fig. 1.10) seen as a resonant enhancement of two-phonon Raman scattering in the vicinity of 1,200 cm^{-1} [70].

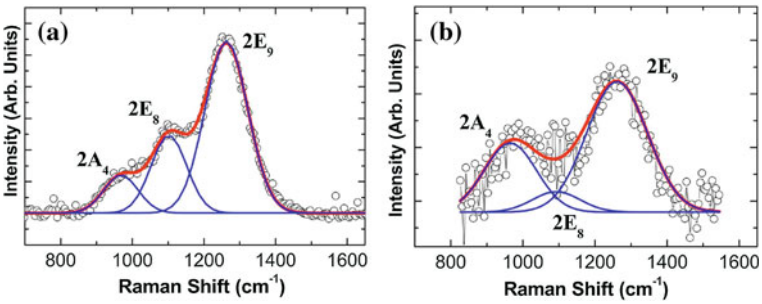

Fig. 1.10 Raman spectrum of bismuth ferritte in the 700–1,600 cm^{-1} wavenumber region. *Solid lines* are fits to three Gaussian functions corresponding to two-phonon replica of the *A*4, *E*8, and *E*9 normal modes in BFO, respectively. **a** Room temperature and **b** $T = 400$ °C above the magnetic transition. From [70]

SHG (the creation of photons with twice the incident light frequency) is observable with an intense light source such as a pulsed laser and follows selection rules based on the materials symmetry. Electric dipole SHG, for example, is allowed only in noncentrosymmetric systems (materials lacking inversion symmetry). It is important to note that inversion symmetry is also broken at surfaces and interfaces. A detailed analysis is needed to separate the individual bulk and surface components of the SHG signal.

The interplay between spin waves and electronic structure in materials leads to the creation of additional bands associated with electronic energy levels which are called magnon sidebands. The large difference in the energy scales between magnons (meV) and electronic levels (eV) makes this direct interaction weak and hence makes magnon sidebands difficult to probe. SHG has been used to successfully measure the magnon sidebands in bismuth ferrite, which are associated with large wave vector multimagnon excitations which linear absorption studies are able to resolve only under high magnetic fields and low temperatures (Fig. 1.11) [71]. Polarized light studies and temperature dependence of these sidebands reveal a spin-charge coupling interaction of the type P_sL_2 between the spontaneous polarization P_s and antiferromagnetic order parameter, L in bismuth ferrite that persists with short-range correlation well into the paramagnetic phase up to high temperatures. These observations suggest a broader opportunity to probe the collective spin-charge-lattice interactions in a wide range of material systems at high temperatures and electronic energy scales using nonlinear optics.

A pump-probe approach has been used to observe ferromagnetic dynamics in ferromagnetic strontium ruthenate [72]. In principle, the dynamics of multiferroic interfaces can be investigated in a similar manner. The main advantage of these optical techniques is that they are a contactless and nondestructive method for studying magnetic, ferroelectric properties and also time-dependent phenomena of surfaces and buried interfaces.

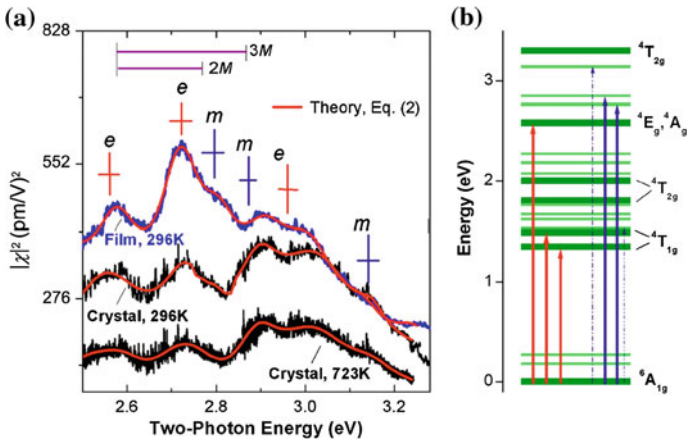

Fig. 1.11 **a** RT SHG spectra obtained in $BiFeO_3$ film (*black*) and bulk single crystal (*blue*). *e* (electronic) and *m* (magnetic) resonances are shown. **b** Electronic energy-level diagram of Fe^{3+} in $BiFeO_3$. *Dark green bars*: energy positions for the *d* to *d* excitations of Fe^{3+} ions. *Light green bars*: energy positions for two- and three-magnon sidebands. *Arrows* indicate the electronic (*red*) and magnon (*blue*) SHG resonances. Broken *blue arrows* suggest multiple possibilities for the 3.14 eV magnon resonance. From [71]

1.5 High-Resolution Electron Microscopy and Spectroscopy

Among the methods available for the investigation of multiferroic materials on the nanoscale and atomic scale are high-resolution electron microscopy (HREM) [73–77]. This method allows direct visualization of the lattice distortion across a multiferroic domain wall by measuring the continuous deviation of a set of planes with respect to the undistorted lattice (exit-wave reconstruction) see Fig. 1.12.

Current, state-of-the-art techniques permit atomic scale resolution at 0.5Å, through aberration-corrected imaging. The exit-wave reconstruction approach eliminates the effects of objective-lens spherical aberrations, and images can be directly interpreted in terms of the projection of the atomic columns. Weak beam transmission electron microscopy (WBTEM) has been used for a quantitative analysis of the thickness fringes that appear on weak beam images of inclined domain walls. By fitting simulated fringe profiles to experimental ones, it is possible to extract the thickness of multiferroic domain walls in a quantitative way. Regarding HRTEM images of domain walls, it has to be taken into account that the samples in these kinds of experiments are very thin (typically a few nm) so that surface pinning of the domain walls could play an important role. The atomic displacements across a typical wall are on the order of 0.02 nm, which makes direct imaging and interpretation still a challenge. HRTEM also offers the possibility of imaging the local polarization dipoles at atomic resolution, thus quantitatively measuring the local polarization and investigating the domain structure [78].

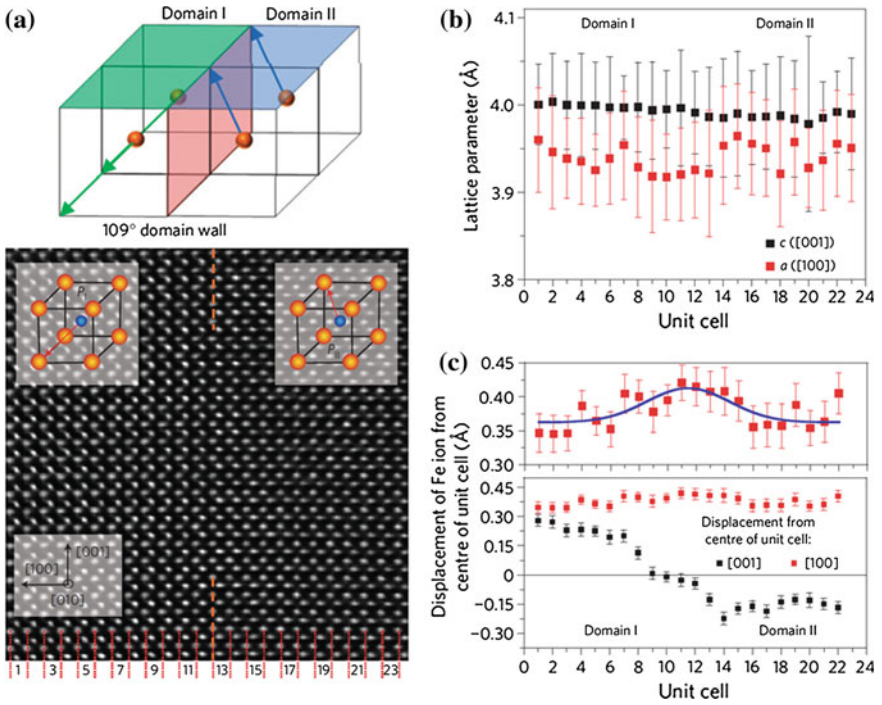

Fig. 1.12 Structural analysis of domain walls in multiferroic bismuth ferrite. **a** Schematic diagram of 109° domain wall and exit-wave-reconstructed HRTEM image of a 109° domain wall imaged along the [010] zone axis. **b** Extracted *a* and *c* lattice parameters for each unit cell across the domain wall. **c** Extracted Fe-ion displacement relative to the Bi lattice for each unit cell across the domain wall. A close-up (*upper panel*) reveals an increase in the component of polarization perpendicular to the domain wall. From [22]

Elemental and electronic structure analysis by Electron-Energy-Loss-Spectroscopy (EELS) has also been applied to the study of domain walls [79–81]. Using high-resolution imaging in an aberration-corrected TEM, the concentration of oxygen in $BaTiO_3$ twin boundaries was measured at atomic resolution. These measurements provide quantitative evidence for a substantial reduction of the oxygen occupancy, i.e., the presence of oxygen vacancies at the boundaries. It was also found that the modified Ti_2O_9 group unit formed reduces the grain boundary energy and provides a way of accommodating oxygen vacancies occurring in oxygen-deficient materials. This type of atomically resolved measurement technique offers the potential to study multiferroic oxide materials in which the electronic properties sensitively depend on the local oxygen content.

1.6 Summary and Outlook

Nanoscale phenomena in multiferroic materials form an exciting and growing field of interest in functional materials. With the current developments surrounding interfaces and nanoscale features like domain walls there are many remaining questions and some new ones. For example the investigation of dynamic conductivity at domain walls is an exciting aspect [82]. This addresses important factors: a possible electric-field induced distortion of the polarization structure at the domain wall; the dependence of conductivity on the degree of distortion; and weak-pinning scenarios of the distorted wall. The domain wall is very likely not a rigid electronic conductor, instead offering a quasi-continuous spectrum of voltage-tunable electronic states [82]. This is different from ferroelectric domains, where switching may give rise to discrete (often only two) conductance levels [18, 19]. The intrinsic dynamics of domain walls and other topological defects are expected not only to influence future theoretical and experimental interpretations of the electronic phenomena, but also pose a possibility to find unique properties of multiferroic domain walls, e.g. magnetization and magnetoresistance within an insulating antiferromagnetic matrix [83], also due to order parameter coupling and localized secondary order parameters. Of obvious future interest is the question of what sets the limits to the current transport behavior at walls: can one "design" the topological structure of the domain wall to controllably induce electronic phase transitions within the wall arising from the correlated electron nature? Is it possible to trigger an Anderson transition by doping of domain walls or straining them? The observation of superconductivity in ferroelastic walls of WO_3 certainly points to various exciting and unexplored areas of domain boundary physics.

The investigation of topological defects beyond the classic domain walls are also a new exciting area of research. Exotic topological defects in nanostructures (vertices, vortices, quadrupoles, etc.) are currently a very active area of research. For example, vortex cores in $BiFeO_3$ have been demonstrated to be dynamic conductors controlled by the coupled response of polarization and electron–mobile-vacancy subsystems with external bias [84].

Experimental results and theoretical investigations in recent years have convincingly demonstrated that certain transition metal oxides and some other materials have dominant properties driven by spatial inhomogeneity. Strongly correlated materials incorporate physical interactions (spin, charge, lattice and/or orbital hybridization), allowing complex interactions between electric and magnetic properties, resulting in ferromagnetic, anti-ferromagnetic phase transitions. Of even higher interest are the hetero-interfaces formed between correlated materials showing new state properties. Domain walls are only one example of "naturally" occurring interfaces in such materials. The challenge is to determine whether such complex interactions can be controlled in those materials or heterointerfaces at sufficiently high speeds and densities to enable new logic device functionality at the nanometer scale. Parameters such as interface energy, switching speed and threshold, tunability, dynamics of the states, and size

dependencies need to be quantified on the nanoscale to determine if domain boundary materials could be employed as a building block for information processing systems.

In summary, we have provided an overview on nanoscale characterization methods for multiferroic materials. The ferromagnetic properties of ferroelectric walls in paramagnetic and antiferromagnetic materials suggest that much more R&D should be done on domain walls in multiferroics as well as for the dynamics of domain walls in these materials [85–87]. Artificially engineered oxide interfaces may pave the way to novel tailored states of matter with a wide range of electronic properties. Many ferroelectric relaxor-like systems nanoscale phase separated materials are interesting as well since they have intrinsic nanodomains. Domain-wall electronics, particularly with ferroelectrics and multiferroics, may become interesting for nanotechnology [88].

Acknowledgements R. R. acknowledges support by the Director, Office of Science, Office of Basic Energy Sciences, Materials Sciences Division of the US Department of Energy under contract No DE-AC02-05CH1123. J. S. acknowledges support by the Australian Research Council through a Future Fellowship (FT110100523).

References

1. M. Imada, A. Fujimori, Y. Tokura, Rev. Mod. Phys. **70**(998), 1039–1263
2. W. Eerenstein et al., Nature **442**, 759 (2006)
3. L.M. Eng, Nanoscale domain engineering and characterization of ferroelectric domains. Nanotechnology **10**, 405 (1999)
4. S.B. Ogale, *Thin Films and Heterostructures for Oxide Electronics* (Springer, NewYork, 2005)
5. A. Ohtomo, D.A. Muller, J.L Grazul, H.Y.Wang, Nature **419**, 378–380 (2002)
6. E. Dagotto, When oxides meet face to face. Science **318**, 1076–1077 (2007)
7. J. Mannhart, D.G. Schlom, Oxide interfaces—an opportunity for electronics. Science **327**, 1607–1611 (2010)
8. H. Yamada et al., Engineered interface of magnetic oxides. Science **395**, 646–648 (2004)
9. P. Zubko, S. Gariglio, M. Gabay, P. Ghosez, J.-M. Triscone, Interface physics in complex oxide heterostructures. Annu. Rev. Cond. Mat. Phys. **2**, 141–165 (2011)
10. S.V. Kalinin et al., Rep. Prog. Phys. **73**, 056502 (2010)
11. A. Gruverman, B.J. Rodriguez, C. Dehoff, J.D. Waldrep, A.I. Kingon, R.J. Nemanich, J.S. Cross, Direct studies of domain switching dynamics in thin film ferroelectric capacitors. Appl. Phys. Lett. **87**, 082902 (2005)
12. B.J. Rodriguez, S. Jesse, A.P. Baddorf, T. Zhao, Y.H. Chu, R. Ramesh, E.A. Eliseev, A.N. Morozovska, S.V. Kalinin, Spatially resolved mapping of polarization switching behavior in nanoscale ferroelectrics. Nanotechnology **18**, 405701 (2007)
13. T. Jungk, A. Hoffmann, E. Soergel, Impact of elasticity on the piezoresponse of adjacent ferroelectric domains investigated by scanning force microscopy. J. Appl. Phys. **102**, 084102 (2007)
14. S. Choudhury et al., The influence of 180° ferroelectric domain wall width on the threshold field for wall motion. J. Appl. Phys. **104**, 084107 (2008)
15. C.-H. Yang, J. Seidel, S.Y. Kim, P.B. Rossen, P. Yu, M. Gajek, Y.-H. Chu, L.W. Martin, M.B. Holcomb, Q. He, P. Maksymovych, N. Balke, S.V. Kalinin, A.P. Baddorf,

S.R. Basu, M.L. Scullin, R. Ramesh, Electric modulation of conduction in multiferroic Ca-doped $BiFeO_3$ films. Nat. Mater. **8**, 485 (2009)
16. N. Balke, S. Jesse, A. Morozovska, E. Eliseev, D. Chung, Y. Kim, L. Adamczyk, R. Garcia, Nanoscale mapping of ion diffusion in a lithium-ion battery cathode. Nat. Nanotechnol. **5**, 749–754 (2010)
17. A. Kumar, F. Ciucci, A.N. Morozovska, S.V. Kalinin, S. Jesse, Nat. Chem. **3**, 707–713 (2011)
18. V. Garcia, S. Fusil, K. Bouzehouane, S. Enouz-Vedrenne, N.D. Mathur, A. Barthelemy, M. Bibes, Nature **460**, 81 (2009)
19. P. Maksymovych, S. Jesse, P. Yu, R. Ramesh, A.P. Baddorf, S.V. Kalinin, Science **324**, 1421 (2009)
20. B.J. Rodriguez, Y.H. Chu, R. Ramesh, S.V Kalinin, Appl. Phys. Lett. **93**, 142901 (2008)
21. Y. Watanabe, Ferroelectrics **349**, 190 (2007)
22. J. Seidel, L.W. Martin, Q. He, Q. Zhan, Y.-H. Chu, A. Rother, M.E. Hawkridge, P. Maksymovych, P. Yu, M. Gajek, N. Balke, S.V. Kalinin, S. Gemming, F. Wang, G. Catalan, J.F. Scott, N.A. Spaldin, J. Orenstein, R. Ramesh, Conduction at domain walls in oxide multiferroics. Nat. Mater. **8**, 229 (2009)
23. J. Seidel, P. Maksymovych, A.J. Katan, Y. Batra, Q. He, A.P. Baddorf, S.V. Kalinin, C.-H. Yang, J.-C. Yang, Y.-H. Chu, E.K.H. Salje, H. Wormeester, M. Salmeron, R. Ramesh, Domain wall conductivity in La-doped $BiFeO_3$. Phys. Rev. Lett. **105**, 197603 (2010)
24. S. Kim et al., Optical index profile at an antiparallel ferroelectric domain wall in lithium niobate. Mater. Sci. Eng., B **120**, 91–94 (2005)
25. T.J. Yang, Direct observation of pinning and bowing of a single ferroelectric domain wall. Phys. Rev. Lett. **82**, 4106–4109 (1999)
26. A. Tselev et al., ACS Nano **4**(8), 4412–4419 (2010)
27. W. Fan, J. Cao, J. Seidel, Y. Gu, J.W. Yim, C. Barrett, K.M. Yu, J. Ji, R. Ramesh, L.Q. Chen, J. Wu, Large kinetic asymmetry in the metal-insulator transition nucleated at localized and extended defects. Phys. Rev. B **83**, 235102 (2011)
28. I. Maggio-Aprile, C. Rennet, A. Erb, E. Walker, O. Fischer, Critical currents approaching the depairing limit at a twin boundary in YBa2Cu3O(7-δ). Nature **390**, 487–490 (1997)
29. A. Wiessner, J. Kirschner, G. Schafer, Th Berghaus, Design considerations and performance of a combined scanning tunneling and scanning electron microscope. Rev. Sci. Instrum. **68**, 3790 (1997)
30. B. Yang, N.J. Park, B.I. Seo, Y.H. Oh, S.J. Kim, S.K. Hong, S.S. Lee, Y.J. Park, Appl. Phys. Lett. **87**, 062902 (2005)
31. R.E. Garcia, B.D. Huey, J.E. Blendell, J. Appl. Phys. **100**, 064105 (2006)
32. Y.P. Chiu, Y.T. Chen, B.C. Huang, M.C. Shih, J.C. Yang, Q. He, C.W. Liang, J. Seidel, Y.C. Chen, R. Ramesh, Y.H. Chu, The evolution of local electronic structure across multiferroic domain walls. Adv. Mat. **23**, 1530 (2011)
33. T. Choi et al., Insulating interlocked ferroelectric and structural antiphase domain walls in multiferroic YMnO3. Nat. Mater. **9**, 253–258 (2010)
34. D. Meier, J. Seidel, A. Cano, K. Delaney, Y. Kumagai, M. Mostovoy, N. A. Spaldin, R. Ramesh, M. Fiebig, Anisotropic conductance at improper ferroelectric domain walls, Nat. Mater. p 284 (2012)
35. B.G. Idlis, M.S. Usmanov, Effect of domain structure on the energy spectrum of narrow-gap ferroelectric semiconductors. Pis'ma Zh. Eksp. Teor. Fiz. **56**, 268 (1992)
36. Y. Xiao, V.B. Shenoy, K. Bhattacharya, Depletion layers and domain walls in semiconducting ferroelectric thin films. Phys. Rev. Lett. **95**, 247603 (2005)
37. T.M.Y. Gureev, A.K. Tagantsev, N. Setter, Structure and energy of charged domain walls in ferroelectrics, in *18th IEEE ISAF Proceedings* (2009)
38. M.L. Scullin et al., Acta Mater. **58**, 457 (2010)
39. Y.-H. Lee, J.-M. Wu, C.-H. Lai, Appl. Phys. Lett. **88**, 042903 (2006)
40. X. Qi, J. Dho, R. Tomov, M.G. Blamire, J.L. MacManus-Driscoll, Appl. Phys. Lett. **86**, 062903 (2005)

41. J.K. Kim, S.S. Kim, W.-J. Kim, A.S. Bhalla, R. Guo, Appl. Phys. Lett. **88**, 132901 (2006)
42. K.T. Ko, M.H. Jung, J.H. Lee, C.S. Woo, K. Chu, J. Seidel, Y.H. Chu, Y.H. Jeong, R. Ramesh, J.H. Park, C.-H. Yang, Concurrent transition of ferroelectric and magnetic ordering around room temperature. Nat. Commun. **2**, 567 (2011)
43. M. Ramirez et al., Appl. Phys. Lett. **94**, 161905 (2009)
44. M.O. Ramirez et al., Appl. Phys. Lett. **92**, 022511 (2008)
45. S.-Y. Yang, J. Seidel, S.J. Byrnes, P. Shafer, C.-H. Yang, M.D. Rossell, P. Yu, Y.-H. Chu, J.F. Scott, J.W. Ager III, L.W. Martin, R. Ramesh, Above band gap voltages from ferroelectric photovoltaic devices. Nat. Nanotechnol. **5**, 143 (2010)
46. J. Seidel, D. Fu, S.-Y. Yang, E. Alarcòn-Lladò, J. Wu, R. Ramesh, J.W. Ager, Efficient photovoltaic current generation at ferroelectric domain walls. Phys. Rev. Lett. **107**, 126805 (2011)
47. J. Seidel, S.-Y. Yang, E. Alarcòn-Lladò, J.W. Ager, R. Ramesh, Nanoscale probing of high photovoltages at 109° domain walls. Ferroelectrics **433**, 123 (2012)
48. J. Zhang, B. Xiang, Q. He, J. Seidel, R. Zeches, P. Yu, S.-Y. Yang, C.-H. Yang, Y.-H. Chu, L.W. Martin, A.M. Minor, R. Ramesh, Large field-induced strain in a lead-free piezoelectric material. Nat. Nanotechnol. **6**, 98 (2011)
49. Y. Heo, B.-K. Jang, K.-E. Kim, C.-H. Yang, J. Seidel, Nanoscale mechanical softening of morphotropic materials, submitted (2014)
50. J. Zhou, M. Trassin, Q. He, N. Tamura, N. Kunz, C. Cheng, J. Zhang, W.-I. Liang, J. Seidel, C. Hsin, Y.-H. Chu, J. Wu, Directed assembly of nanoscale phase variants in highly strained $BiFeO_3$ thin films. J. Appl. Phys. **112**, 064102 (2012)
51. J. Seidel, M. Trassin, Y. Zhang, P. Maksymovych, T. Uhlig, P. Milde, D. Koehler, A.P. Baddorf, S.V. Kalinin, L.M. Eng, X. Pan, R. Ramesh, Electronic properties of isosymmetric phase boundaries in highly strained Ca-doped $BiFeO_3$. Adv. Mater. (2014)
52. Q. He, Y.H. Chu, J.T. Heron, S.Y. Yang, W.I. Laing, C.Y. Kuo et al., Electrically controllable spontaneous magnetism in nanoscale mixed phase multiferroics. Nat. Commun. **2**, 225 (2011)
53. K.T. Ko, M.H. Jung, Q. He, J.H. Lee, C.S. Woo, K. Chu, J. Seidel, B.-G. Jeon, Y.S. Oh, K.H. Kim, W.-I. Liang, H.-J. Chen, Y.H. Chu, Y.H. Jeong, R. Ramesh, J.-H. Park, C.-H. Yang, Concurrent transition of ferroelectric and magnetic ordering around room temperature. Nat. Commun. **2**, 567 (2011)
54. K.I. Kugel, D.I. Khomskii, The Jahn-Teller effect and magnetism: transition metal compounds. Sov. Phys. Usp. **2**(5), 231–256 (1982)
55. Ikeda et al., submitted (2013)
56. J. H. Lee et al., Phase separation and electrical switching between two isosymmetric multiferroic phases in tensile strained $BiFeO_3$ thin films. Phys. Rev. B **89**, 140101(R) (2014)
57. T. Zhao, A. Scholl, F. Zavaliche, K. Lee, M. Barry, A. Doran et al., Electrical control of antiferromagnetic domains in multiferroic $BiFeO_3$ films at room temperature. Nat. Mater. **5**, 823–829 (2006)
58. Y.H. Chu, L.W. Martin, M.B. Holcomb, M. Gajek, S.J. Han, Q. He et al., Electric-field control of local ferromagnetism using a magnetoelectric multiferroic. Nat. Mater. **7**, 478 (2008)
59. I. Sosnowska et al., J. Phys. C **15**, 4835 (1982)
60. I. Sosnowska et al., Appl. Phys. A **74**, 1040 (2002)
61. T. Stevenson et al., J. Magn. Magn. Mater. **322**, L64 (2010)
62. H. Bea, M. Bibes, S. Petit et al., Structural distortion and magnetism of $BiFeO_3$ epitaxial thin films: A Raman spectroscopy and neutron diffraction study. Phil. Mag. Lett. **87**, 165–174 (2007)
63. D. Lebeugle et al., Phys. Rev. Lett. **100**, 227602 (2008)
64. Y. Yamasaki et al., Phys. Rev. Lett. **98**, 147204 (2007)
65. M. Kenzelmann et al., Phys. Rev. Lett. **98**, 267205 (2007)
66. P.G. Radaelli et al., Phys. Rev. Lett. **101**, 067205 (2008)
67. G.P. Felcher et al., Phys. B **297**, 87 (2001)

68. D. Sando et al., Crafting the magnonic and spintronic response of $BiFeO_3$ films by epitaxial strain. Nat. Mater. **12**, 641 (2013)
69. J.-M. Hu et al., Nat. Commun. **2**, 553 (2011)
70. M.O. Ramirez, M. Krishnamurthi, S. Denev, A. Kumar, S.-Y. Yang, Y.-H. Chu, E. Saiz, J. Seidel, A.P. Pyatakov, A. Bush, D. Viehland, J. Orenstein, R. Ramesh, V. Gopalan, Two-phonon coupling to the antiferromagnetic phase transition in multiferroic $BiFeO_3$. Appl. Phys. Lett. **92**, 022511 (2008)
71. M.O. Ramirez, A. Kumar, S. Denev, N. Podraza, X.S. Xu, R.C. Rai, Y.-H. Chu, J. Seidel, L. Martin, S.-Y. Yang, E. Saiz, J.F. Ihlefeld, S. Lee, S.W. Cheong, D.G. Schlom, R. Ramesh, J. Orenstein, J.L. Musfeldt, V. Gopalan, Magnon sidebands in bismuth ferrite probed by nonlinear optical spectroscopy. Phys. Rev. B **79**, 224106 (2009)
72. M.C. Langner, C.L.S. Kantner, Y.-H. Chu, L.W. Martin, P. Yu, J. Seidel, R. Ramesh, J. Orenstein, Observation of ferromagnetic resonance in $SrRuO_3$ by the time-resolved magneto-optical Kerr effect. Phys. Rev. Lett. **102**, 177601 (2009)
73. E.K.W. Goo et al., J. Appl. Phys. **52**, 2940 (1981)
74. L.A. Bursill, J.L. Peng, D. Feng, Philos. Mag. A **48**, 953 (1983)
75. S. Stemmer et al., Philos. Mag. A **71**, 713 (1995)
76. H. Lichte, Ultramicroscopy **93**, 199 (2002)
77. C.L. Jia, Science **299**, 870 (2003)
78. C.-L. Jia, S.-B. Mi, K. Urban, I. Vrejoiu, M. Alexe, D. Hesse, Nat. Mater. **7**, 57 (2008)
79. C.L. Jia, K. Urban, Science **303**, 2001 (2004)
80. K. Urban et al. (ed.), *Advances in Imaging and Electron, Physics*, vol. 153, (Elsevier, New York, 2008), p. 439
81. M. D. Rossell et al., Atomic structure of highly strained $BiFeO_3$ thin films. Phys Rev Lett. **108**, 047601 (2012)
82. J. Maksymovych, Y.-H. Seidel, A. Chu, P. Baddorf, L.-Q. Wu, S. Chen, V. Kalinin, R. Ramesh, Dynamic conductivity of ferroelectric domain walls. Nano Lett. **11**, 1906 (2011)
83. Q. He, C.-H. Yeh, J.-C. Yang, G. Singh-Bhalla, C.-W. Liang, P.-W. Chiu, G. Catalan, L. W. Martin, Y.-H. Chu, J. F. Scott, R. Ramesh, Magnetotransport at Domain Walls in $BiFeO_3$. Phys. Rev. Lett. **108**, 067203 (2012)
84. N. Balke, B. Winchester, W. Ren, Y.H. Chu, A.N. Morozovska, E.A. Eliseev, M. Huijben, R.K. Vasudevan, P. Maksymovych, J. Britson, S. Jesse, I. Kornev, R. Ramesh, L. Bellaiche, L.Q. Chen, S.V. Kalinin, Enhanced electric conductivity at ferroelectric vortex cores in $BiFeO_3$. Nat. Phys. **8**, 81(2012)
85. A.V. Goltsev, R.V. Pisarev, Th Lottermoser, M. Fiebig, Phys. Rev. Lett. **90**, 177204 (2003)
86. M. Daraktchiev, G. Catalan, J.F. Scott, Landau theory of domain wall magnetoelectricity. Phys. Rev. B **81**, 224118 (2010)
87. V. Skumryev, V. Laukhin, I. Fina, X. Martı, F. Sanchez, M. Gospodinov, J. Fontcuberta, Magnetization reversal by electric-field decoupling of magnetic and ferroelectric domain walls in multiferroic-based heterostructures. Phys. Rev. Lett. **106**, 057206 (2011)
88. G. Catalan, J. Seidel, R. Ramesh, J.F. Scott, Domain wall nanoelectronics. Rev. Mod. Phys. **84**, 119 (2012)

http://www.springer.com/978-3-642-55374-5

Mesoscopic Phenomena in Multifunctional Materials
Synthesis, Characterization, Modeling and Applications
Saxena, A.; Planes, A. (Eds.)
2014, XIV, 316 p. 167 illus., 52 illus. in color., Hardcover
ISBN: 978-3-642-55374-5